Thesis for the degree of Licentiate of Engineering

Multidisciplinary Design of Transonic Fans for Civil Aeroengines

Oliver Sjögren

Department of Mechanics and Maritime Sciences
CHALMERS UNIVERSITY OF TECHNOLOGY
Göteborg, Sweden 2023

Multidisciplinary Design of Transonic Fans for Civil Aeroengines
Oliver Sjögren

Licentiatavhandlingar vid Chalmers tekniska högskola
Technical report No. 2023:11

Department of Mechanics and Maritime Sciences
Chalmers University of Technology
SE–412 96 Göteborg, Sweden
Telephone + 46 (0) 31 – 772 1000

Typeset by the author using LaTeX.

Printed by Chalmers Reproservice
Göteborg, Sweden 2023

Abstract

Multidisciplinary Design of Transonic Fans for Civil Aeroengines
Oliver Sjögren
Mechanics and Maritime Sciences
Fluid Dynamics
Chalmers University of Technology

For current state-of-the-art turbofan engines the bypass section of the fan stage alone provides the majority of the total thrust in cruise and the size of the fan has a considerable effect on overall engine weight and nacelle drag. Thrust requirements in different parts of the flight envelope must also be satisfied together with sufficient margins towards stall. A complex set of system requirements and objectives, combined with component technology of high maturity level, demands performance predictions with higher accuracy that are sensitive to more detailed design features at an early conceptual design phase. Failing to meet these demands may result in a sub-optimal choice of aircraft-engine system architecture. The emphasise of this thesis work will be on fan-stage design and performance prediction in terms of aerodynamic efficiency and stability. The aspect of accuracy when it comes to establishing engine cycle performance for existing state-of-the-art technology based on open literature data is undertaken in the first paper. In the second paper a strategy to expand the parameter interdependencies of a fan-stage performance model with a multidisciplinary perspective is explored. The resulting model is integrated into an engine systems model and coupled with a simplified weight model to investigate the trade-off between weight and specifc fuel consumption. Results implied that being able to predict the rotor solidity required to maintain a given average blade loading - in addition to stage efficiency - is of high importance.

Keywords: Jet propulsion, Transonic fan stage design, Turbofan performance, Performance optimization, Design of experiment, Stochastic sensitivity analysis, Multidisciplinary design

Acknowledgments

Firstly, I would like to thank Anders Lundbladh at GKN Aerospace Trollhättan for the insights and expertise that you so willingly share. Your support is invaluable. I would also like to thank my supervisor at Chalmers Carlos Xisto for guiding me through this endeavour, giving me constructive feedback and for raising my spirit during challenging times. Furthermore I would like to thank my examiner Tomas Grönstedt for giving me this opportunity in the first place and for being a pillar of strength when necessary.

I also want to extend a heartfelt gratitude to my family for their patience, love, and support. Lastly I want to thank my colleagues at the Fluid Dynamics division and in particular my fellow PhD students in the Turbomachinery and Aeroacoustics group for brightening up the day creating a great working environment.

This work was carried out at the division of Fluid Dynamics, department of Mechanics and Maritime Sciences at Chalmers University of Technology as part of the FANG project (Fan Alternatives For Next Generation engines). Funding was provided by the Swedish National Aviation Engineering Research Program, NFFP, supported by Swedish Armed Forces, the Swedish Defense Materiel Administration, Swedish Governmental Agency for Innovation Systems (VINNOVA) and GKN Aerospace.

Oliver Sjögren
Göteborg, August 2023

List of Publications

This thesis is based on the following appended papers:

Paper 1. Oliver Sjögren, Carlos Xisto and Tomas Grönstedt. *Estimation of Design Parameters and Performance for a State-of-the-Art Turbofan.* Proceedings of the ASME Turbo Expo 2021: Turbomachinery Technical Conference and Exposition. Volume 1: Aircraft Engine; Fans and Blowers; Marine; Wind Energy; Scholar Lecture. Virtual, Online. June 7–11, 2021. V001T01A013. ASME. https://doi.org/10.1115/GT2021-59489

Paper 2. Oliver Sjögren, Tomas Grönstedt, Carlos Xisto, Anders Lundbladh. *Fan Stage Design and Performance Optimization for Low Specific Thrust Turbofans.* Submitted to the International Journal of Turbomachinery, Propulsion and Power.

Nomenclature

Roman symbols

B	–	Annulus blockage factor
c	–	Chord
D	–	Lieblein's diffusion factor
D_{eq}	–	Lieblein's equivalent diffusion factor
c_p	–	Specific heat at constant pressure
h	–	Specific enthalpy
H	–	Boundary layer shape factor
i	–	Incidence angle
k_t	–	Eddy thermal conductivity
l	–	Annulus height
m	–	Meridional coordinate
$\dot{m}$	–	Mass flow rate
n	–	Coordinate in normal direction
P	–	Pressure
q	–	Quasi-orthogonal coordinate
r	–	Radial coordinate
Re	–	Reynolds number
s	–	Specific entropy
t_{max}	–	Maximum airfoil thickness
T	–	Temperature
U	–	Blade speed
V	–	Velocity in stationary frame
W	–	Velocity in relative frame
z	–	axial coordinate

Greek symbols

α	–	Flow angle in stationary frame
α'	–	Blade metal angle
γ	–	Quasi-orthogonal inclination, or specific heat ratio
δ	–	Deviation
δ^*	–	Boundary layer displacement thickness
ϵ	–	Tip clearance
ϵ^*_{gal}	–	Gallimore's mixing parameter
θ	–	Tangential coordinate, or camber angle
θ_{ew}	–	Endwall boundary layer momentum thickness

θ_w	–	Trailing edge wake momentum thickness
κ	–	Streamline curvature
μ_t	–	Eddy viscosity
ξ	–	Stagger angle
ρ	–	Density
σ	–	Solidity
ϕ	–	Streamline slope
$\overline{\omega}$	–	Total loss coefficient
ω_{ew}	–	Endwall loss coefficient
ω_p	–	Profile loss coefficient
ω_{shk}	–	Shock loss coefficient

Subscripts

0	–	Stagnation property
1	–	Inlet station
2	–	Outlet station
a	–	Upstream
b	–	Downstream
h	–	Hub
m	–	Meridional component
n	–	Normal component
q	–	Component in the quasi-orthogonal direction
r	–	Radial component
t	–	Tip, or casing
z	–	Axial component
θ	–	Tangential component

Acronyms

AR	–	Aspect ratio
SLC	–	Streamline curvature
QO	–	Quasi-orthogonal
DCA	–	Double circular arc

Contents

Abstract iii

Acknowledgments v

List of Publications vii

List of Acronyms ix

I Introductory Chapters 1

1 Introduction 3
1.1 Aim . . . 5

2 Methods 7
2.1 Streamline curvature modelling . . . 7
2.1.1 Assumptions and governing equations . . . 7
2.1.2 Loss and deviation . . . 10
2.1.3 Blockage and spanwise mixing . . . 13

3 Summary of Papers 15
3.1 Paper 1 . . . 15
3.1.1 Methodology . . . 15
3.1.2 Summary and discussion . . . 15
3.2 Paper 2 . . . 16
3.2.1 Methodology . . . 16
3.2.2 Summary and discussion . . . 16

4 Concluding Remarks 19
4.1 Summary . . . 19
4.2 Future work . . . 19

Bibliography 21

II Appended papers **23**

1 Estimation of Design Parameters and Performance for a State-of-the-Art Turbofan **25**

2 Fan Stage Design and Performance Optimization for Low Specific Thrust Turbofans **37**

Part I

Introductory Chapters

Chapter 1

Introduction

In regards to the fan stage in a turbofan engine of a commercial jet, extensive efforts have been put into improving their aerodynamic and mechanical properties over a period of more than 50 years. During this time, method developments and improvements in computing power have progressively allowed for effects of more detailed geometric features and - eventually - highly 3-dimensional blade shapes to be investigated both structurally and aerodynamically. Thanks to the advent of improved materials and manufacturing techniques, the aerodynamic benefit of more complex shapes can today be achieved reliably. Lighter structures and fan blades have also enabled larger diameter fans with reduced pressure ratio in favour of higher propulsive efficiency. An increase in diameter over time can be observed when comparing available engines for aircraft of similar certified take-off weight as shown in the upper part of Figure 1.1.

In the early days of development of axial flow compressors and fans for aircraft propulsion, the desire for compact and lightweight engines led most designers at the time to adopt configurations with many slender high aspect ratio blades. The aerodynamic benefits of low aspect ratio blades were however underestimated and engine manufacturers eventually started to transition to designs with fewer wide-chord blades [1]. The transition was pioneered by Rolls Royce that successfully updated their RB211 engine with a 22 wide-chord blade fan stage, replacing the previous design with 33 high aspect ratio blades and eliminating the need for a mid-span shroud. This is highlighted in the lower half of Figure 1.1 together with illustrations showing the evolution of fan blade designs of the CFM engine family. A clear trend from slender and straight blades to wide-chord blades with a high degree of sweep can be observed.

Introducing a speed reduction gearbox allowing the fan and the low-pressure turbine to be designed at their optimal speeds independently of one another can enable further improvements in fuel burn and noise reduction. With the first successful application by Pratt & Whitney with the PW1000G engine family paving the way and Rolls Royce investing heavily into the technology with the UltraFan development program - geared turbofan architectures are now considered the more promising choice over direct driven fans for the next generation engines.

With fan stages growing increasingly larger and the thrust generation of the

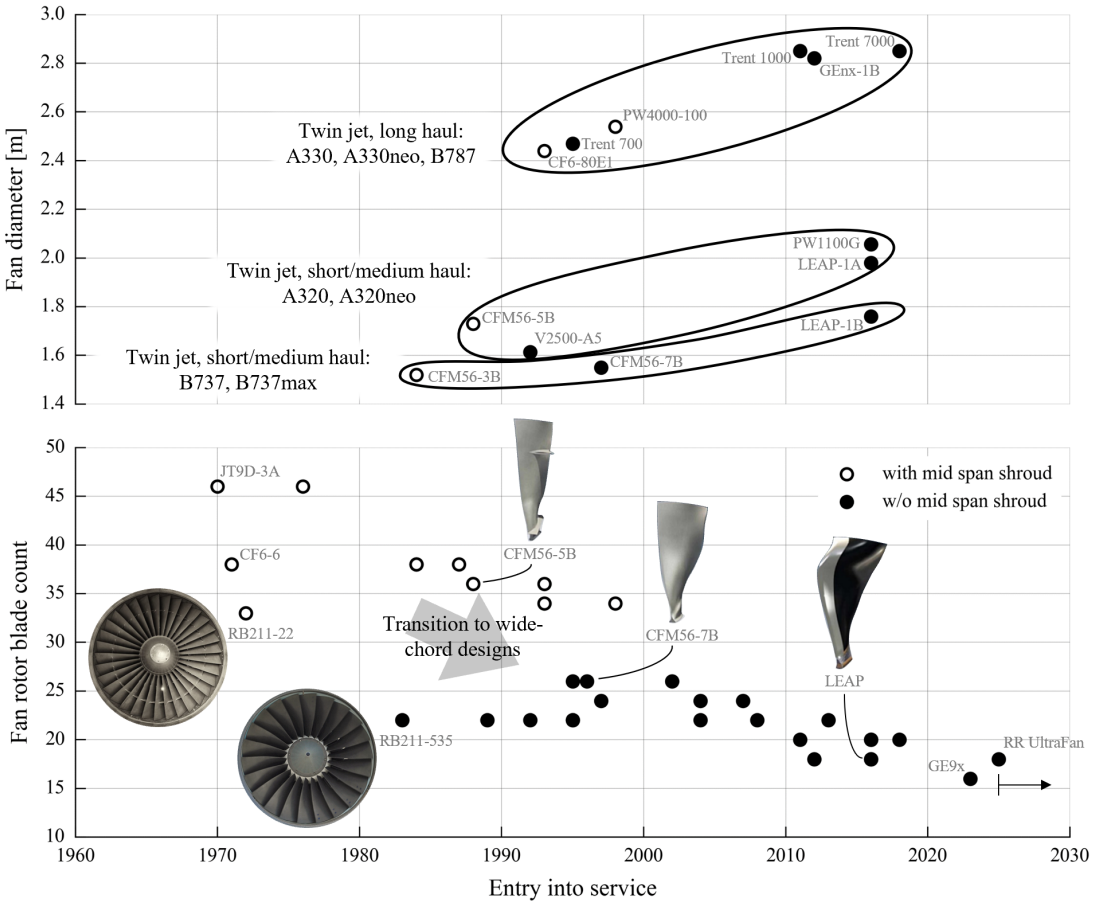

Figure 1.1: Evolution of fan diameter and rotor blade count for commercial jet turbofans. Fan diameter compared between available engines for twin jets of similar certified take-off weight.

bypass flow becoming an even more dominant part of the overall thrust, the trade-off between size, weight, and aerodynamic performance of the fan will be ever more important to consider during the initial conceptual design and analysis of the aircraft as a whole and its mission. In light of recent research on altitude effects from aviation, simply reducing carbon emissions for a fixed mission is not a sufficient objective when considering the overall environmental impact. For a design choice to be deemed justifiable from an environmental as well as economic perspective, it would be of interest to evaluate its effect on cost and the environment during multiple representative use case scenarios. When it comes to commercial jet engines, one particular engine model is rarely used for a single mission alone, but for a wide variety of mission profiles and often for different aircraft models. In order to fit the needs of the market and at the same time allow for necessary altitude changes to avoid weather and potentially contrails formation, operational flexibility has to be considered as well. All in all this results in a complex set of system-level requirements and objectives. Additionally, as component technology level matures, margins for further improvement typically decrease. It is therefore essential to find the “sweet”

spot in terms of model complexity so that key mechanisms and parameter interactions can be represented with just enough accuracy with minimal computational cost in an initial system-level analysis. Failing to do so may result in a sub-optimal choice of system architecture.

1.1 Aim

This thesis and the work presented within is aimed towards fan-stage conceptual design with a main focus on aero -thermodynamic performance, but approached from a multidisciplinary perspective. One part of the thesis is dedicated to establish engine cycle performance for state-of-the-art technology based on publicly available data and asses the uncertainty in the prediction. The focus of the other part is to develop a strategy to increase the coupling between fan stage conceptual design and system level analysis starting with the engine performance and weight and preparing for later integration into an aircraft conceptual design and mission analysis framework. The aim can further be broken down into the following:

- Acquire state-of-the-art engine performance data from public sources.
- Develop an inverse design procedure to match publicly available data to engine cycle performance models and thereby establish a baseline for state-of-the-art technology.
- Estimating the uncertainty of the performance predictions from the inverse design procedure by means of stochastic sensitivity analysis.
- Determine relevant fan stage parameter interdependencies - to be included into a system level analysis - based on guidelines from available literature and first principles.
- Develop a strategy to extract a meaningful representation of said parameter interdependencies from a higher order physics based model of fan stage aero-thermodynamic performance.
- Demonstrate the strategy using a streamline curvature model as a proxy for a high order high fidelity model and integrate the resulting low order fan stage performance model into an engine model.
- Perform an optimization study on the engine model to demonstrate a use case scenario.
- Extend existing framework for aircraft design and mission analysis.
- Use open source data to generate a baseline aircraft model representing a state-of-the-art commercial short-to-medium twin jet.
- Parameterize detailed fan blade and flow passage geometry.

Chapter 2

Methods

2.1 Streamline curvature modelling

The streamline curvature method is a widely used tool for early conceptual design and analysis of turbomachinery components. The method presented here is one based on Denton's formulation [2] and implemented in the commercial software SC90C by PCA Engineering, a code originally developed by Dunham and Ginder [3]. A brief overview of the method in general and the underlying assumptions are described together as well as the implemented correlation's for loss, deviation, endwall blockage and spanwise mixing. Implementation specific details that are not disclosed in the software manual have not been considered. For a more detailed description of the general method the reader is referred to papers by Denton, Novak, and Novak and Hersay [2], [4], [5].

2.1.1 Assumptions and governing equations

In turbomachinery applications it can sometimes be practical to express the governing equations of compressible flow in terms of a natural coordinate system. The natural coordinate system usually employed is here denoted (θ, m, n) and is related to a cylindrical coordinate system (θ, z, r) with its reference axis being the axis of rotation of the turbomachinery component. For a given point in the cylindrical coordinate system with a streamline passing through it, the meridional coordinate m is measured along the projection of the streamline onto the $r-z$ plane - also called the meridional plane. The normal coordinate n is consequently measured along a direction normal to the streamline in the meridional plane and θ being the tangential coordinate. An illustration of the natural coordinate system in reference to the cylindrical coordinate system in the meridional plane is shown in Figure 2.1.

The fundamental assumptions underlying the streamline curvature method is that the flow is steady-state, adiabatic, inviscid, and axially symmetric. As a consequence of the axial symmetry, the streamsurfaces can be represented by concentric surfaces of revolution and the flow field can be solved for in the meridional plane alone. In general it is known that streamsurfaces can twist as they pass through a blade row, but for regions in between blade rows this can be considered a reasonable

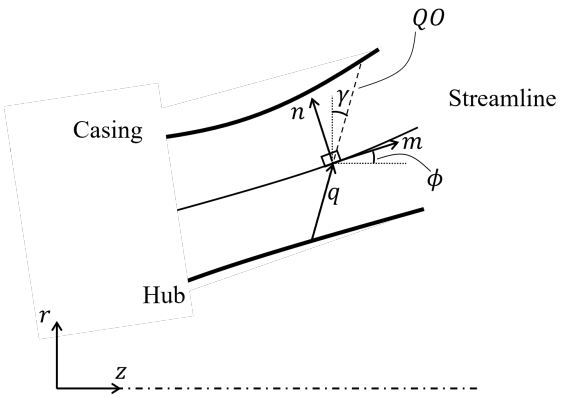

Figure 2.1: Coordinate system in the meridional plane for the streamline curvature method.

assumption [6]. Assuming that the streamsurfaces are known, the acceleration of a fluid particle in the normal direction n can then be expressed in terms of the curvature of the streamline in the meridional plane. However, since the locations of the streamsurfaces are a part of the solution as well, the equation of motion is instead expressed along a quasi-orthogonal coordinate q. Quasi-orthogonal lines QO can then be specified a-priori thus requiring only the coordinate q to be determined. With the notation and sign-convention as illustrated in Figure 2.1, the acceleration of a fluid-particle in the q direction can be expressed accordingly

$$\frac{DV_q}{Dt} = V_m \frac{\partial V_m}{\partial m} \sin(\phi + \gamma) + \kappa_m V_m^2 \cos(\phi + \gamma) - \frac{V_\theta^2}{r} \cos\gamma, \tag{2.1}$$

where κ_m is the curvature of the meridional streamline defined as $\kappa_m = \partial\phi/\partial m$, ϕ is the slope of the meridional streamline and γ is the angle between the quasi-ortogonal line and the $r - \theta$ plane. Applying the momentum equation in the q direction neglecting any body forces and viscous effects gives

$$\frac{DV_q}{Dt} = -\frac{1}{\rho}\frac{\partial P}{\partial q}. \tag{2.2}$$

Together with the Clausius-Gibbs equation relating the pressure gradient to gradients in entropy and enthalpy accordingly

$$-\frac{1}{\rho}\frac{\partial P}{\partial q} = T\frac{\partial s}{\partial q} - \frac{\partial h}{\partial q} \tag{2.3}$$

and the definition of total enthalpy $h_0 = h + V^2/2$, equation 2.1 and 2.2 can be combined to yield

$$V_m \frac{\partial V_m}{\partial q} - \kappa_m V_m^2 \cos(\phi + \gamma) - V_m \frac{\partial V_m}{\partial m} \sin(\phi + \gamma) + \frac{V_\theta}{r}\frac{\partial (rV_\theta)}{\partial q} = \frac{\partial h_0}{\partial q} - T\frac{\partial s}{\partial q}. \tag{2.4}$$

Equation 2.4 representing the normal momentum equation is the foundation for the streamline curvature method. Provided values of curvature and slope of streamlines

at given q coordinates along a quasi-orthogonal, as well as distributionas of total enthalpy, entropy, tangential velocity and the meridional velocity gradient $\partial V_m/\partial m$, the distribution of meridional velocity V_m along the quasi-ortogonal can be solved for numerically. For the solution to be unique, an additional condition on the magnitude of V_m has to be applied. This is accomplished by requiring that the density weighted meridional velocity integrated over the annulus equals a given mass flow rate.

$$\dot{m} = 2\pi \int_{QO} \rho V_m \cos(\phi + \gamma) r B dq \tag{2.5}$$

The effect of endwall blockage have been included in Eq. 2.5 through the parameter B where for ideal flows B is equal to unity.

In order to relate the entropy and the total enthalpy from one quasi-orthogonal to another, energy conservation and losses have to be considered. It is well known that for inviscid and adiabatic flow in the absence of shock waves, the entropy of a moving fluid particle stays constant. For steady-state flow this means that entropy is constant along streamlines. Although, some more general inviscid methods can cope with strong shocks and even account for viscous effects through additional body-force terms [7]. For the streamline curvature method, imposing changes in entropy between quasi-orthogonals - due to shock losses and viscous losses - is still possible, but the local effects on the flow field from streamwise derivatives of entropy may are not properly taken into account.

It can further be shown that if the flow is inviscid, adiabatic and steady, there can be no change in stagnation enthalpy along a streamline either [8]. This is true for an inertial frame of reference and is valid for stationary blade rows and regions outside of blade rows. Changing to a frame of reference that rotates with the rotor blade row - such that the flow field can be treated as steady-state - it can be shown that rothalpy $I = h + W^2/2 - U^2/2$ is the conserved quantity along streamlines instead [9]. It can also be shown that a change in the angular momentum of the flow over the rotor blade row - in a frame of reference rotating with the blade row - requires a change in total enthalpy in the stationary frame of reference if rothalpy is to be conserved. A change in total enthalpy from a rotor inlet to a rotor outlet, can therefore be achieved in a steady-state analysis by a simple switch in frame of reference. However, for the flow to be treated as steady-state in each frame of reference one has to assume that circumferential non-uniformities in total and static pressure, observed by one blade row due to an adjecent blade row, decays in the distance between them. This is a common assumption for methods far more sophisticated than the streamline curvature method. In general, streamwise gradients of total enthalpy (or rothalpy for a rotor blade row) in a viscous flow will also be a consequence of turbulent mixing that will cause dissipation of momentum and heat across streamlines. For a streamline curvature method, changes in total enthalpy between quasi-orthogonals due to mixing can be included, but may require additional equations for streamwise energy, streamwise momentum and tangential momentum to be solved for to get satisfying results [10].

By equation 2.5 continuity is fulfilled between quasi-orthogonals on an overall basis as long as the same total mass flow rate is specified. This however does not imply

that continuity is fulfilled for each streamsheet (a region bounded by two adjacent streamsurfaces). Continuity for each streamsheet can be fulfilled by requiring a mass flow fraction for each streamsheet in addition to the overall mass flow. Based on the required mass flow between streamlines the position where the streamlines intersect the quasi-orthogonal lines can be updated [9]. From the updated coordinates of each streamline, estimations of streamline curvature κ_m and slope ϕ can be updated as well.

It can be shown that the tangential momentum equation for axially symmetric, time-steady, inviscid flow, in the absence of any body force terms, reduces to constant angular momentum along a streamline [6].

$$\frac{\partial(rV_\theta)}{\partial m} = 0 \tag{2.6}$$

Constant angular momentum is assumed in regions outside of blade rows to relate the tangential velocity at an upstream quasi-orthogonal to a downstream one. A change in angular momentum due to forces exerted by the blades in a blade row, can be modelled in various ways. In case of SC90C, correlations based on linear cascade data are available to relate inlet flow angles to outlet flow angles and losses, expressed in a blade-row-relative frame of reference. The correlations relevant for the purpose of this thesis work are presented in the following sub-sections.

2.1.2 Loss and deviation

In this section, a brief overview of the loss modelling implemented in SC90C is presented. A more detailed description can be found in the papers by Wright and Miller [11] and Miller and Wasdell [12]. According to this method, the blade row total pressure loss is calculated as the sum of three loss sources, namely the profile, endwall and shock loss. The correlations are based on the pressure loss coefficient, which is expressed as the total pressure difference from blade row inlet to outlet divided by the dynamic pressure as presented in Eq. 2.7. Inlet and outlet of a single blade row are from here on represented by Station 1 and 2, respectively.

$$\omega = \frac{P_{01} - P_{02}}{P_{01} - P_1}. \tag{2.7}$$

A description of the correlation for deviation and the correlations linked to each of the loss sources is provided in the following paragraphs. Unless specified otherwise, the stagnation properties, velocities and flow angles are defined relative to a blade section frame of reference.

Outlet flow angle for a given airfoil geometry is calculated as $\alpha_2 = \alpha_2' + \delta$, where δ is the trailing edge deviation and the primed variable α_2' represents the trailing edge metal angle. Deviation is calculated by first estimating its value at a reference incidence value corresponding to the minimum loss condition for the given airfoil geometry. The deviation for an arbitrary incidence angle $i = \alpha_1 - \alpha_1'$ is then obtained from generalized curves relating a change in incidence from the reference value to a corresponding change in deviation. The reference deviation is correlated using

a modified form of Carter's rule that depends on the camber angle, solidity, axial velocity density ratio, maximum thickness to chord ratio and stagger angle.

$$\delta = 1.13\left(\frac{\theta}{\sqrt{\sigma}} + 3\right) f_1(\xi) + \left(\frac{\rho_1 V_{z1}}{\rho_2 V_{z2}} - 1.0\right) f_2(\xi) + \left(\frac{t_{max}}{c} - 0.05\right) f_3(\xi) + 0.8, \quad (2.8)$$

where f_1, f_2 and f_3 are just functions of the blade stagger ξ. Since the correlations presented here are used for double circular arc (DCA) profiles, the stagger angle is given by the leading and the trailing edge metal angles alone according to

$$\xi = \frac{(\alpha_1' - \alpha_2')}{2}. \quad (2.9)$$

The change in tangential velocity from the inlet to the outlet of a blade-row can then be obtained with the flow angles defined as $\alpha = \tan^{-1}(V_\theta / V_m)$.

Profile loss is first determined for the minimum loss incidence using Liebleins pressure loss coefficient [13],

$$\omega_p = 2\frac{\theta_w}{c}\frac{\sigma}{\cos\alpha_2}\left(\frac{V_2}{V_1}\right)^2, \quad (2.10)$$

where the wake momentum thickness per chord θ_w/c is a function of the inlet relative Mach number and Lieblein's equivalent diffusion factor D_{eq} corrected for thickness-to-chord effects. The correlation is established for double circular arc (DCA) airfoils with the equivalent diffusion factor expressed accordingly

$$D_{eq} = \frac{V_1}{V_2}\left\{1 + \frac{V_2}{V_1} + \left[0.1 + \frac{t_{max}}{c}\left(10.116 - 34.25\ \frac{t_{max}}{c}\right)\right]\frac{V_{\theta 1} - V_{\theta 2}}{\sigma V_1}\right\} + 1. \quad (2.11)$$

The profile loss at an arbitrary incidence angle is calculated from the estimated incidence angle at minimum loss, choke and stall condition. The correlation uses generalized curves relating the change in incidence from the minimum loss value to an associated increase in profile loss.

Endwall loss is introduced to take into account effects associated with the endwall boundary layer itself and interactions between the endwall and the blade boundary layer. Wright and Miller [11] correlate these effects with aspect ratio, blade loading and tip clearance on a meanline basis. The implementation in SC90C is expanded to account for 2D flow conditions by considering a parabolic distribution along the span. The undistributed endwall loss coefficient is defined in Eq. 2.12, where the empirical coefficients were calibrated against data for single and multistage compressors, as presented in [11].

$$\omega_{ew} = \left(\frac{V_2}{V_1}\right)^2 \frac{1}{AR} f(D, \epsilon/c), \quad (2.12)$$

The effects of blade loading is considered through Lieblein's diffusion factor [14] defined accordingly,

$$D = 1 - \frac{V_2}{V_1} + \frac{1}{2\sigma}\left(\frac{r_1 V_{\theta 1} - r_2 V_{\theta 2}}{r_1 V_1}\right). \quad (2.13)$$

Shock loss is related to the pressure losses due to shock wave formation within the blade passage when the inlet relative Mach number exceed the critical Mach number. This is estimated through a theoretical loss model introduced by Schwenk et al. [15]. The resulting pressure loss coefficient is calculated from the total pressure recovery over a normal shock estimated from simple one-dimensional relations for a perfect gas.

$$\omega_{shk} = \frac{1 - P_{0b}/P_{0a}}{1 - P_1/P_{01}}.. \tag{2.14}$$

$$\frac{P_{0a}}{P_{0b}} = \left[\frac{(\gamma+1)M_a^2}{(\gamma-1)M_a^2+2}\right]^{\frac{\gamma}{1+\gamma}} \left[\frac{\gamma+1}{2\gamma M_a^2-(\gamma-1)}\right]^{\frac{\gamma}{1+\gamma}}. \tag{2.15}$$

Here γ is the ratio of specific heat and M_a a representative passage Mach number. As illustrated in Figure 2.2, the total pressure immediately before and after the passage shock wave is denoted P_{0a} and P_{0b} respectively. For this purpose the passage Mach number in Eq. 2.15 is taken as the average between the relative inlet Mach M_1 number and the peak suction surface Mach number M_{ss} estimated for DCA cascades [15]. Estimations of M_{ss} in this procedure depends on the inlet Mach number itself, the inlet flow angle, airfoil camber, airfoil stagger, solidity, maximum profile thickness to chord ratio, and leading edge radius. The implementation in SC90C does not estimate the peak suction Mach number for supercritical inlet Mach numbers below 1.0. For an inlet Mach number between 0.8 and 1.0, the shock loss is calculated with $M_1 = 1.0$ regardless. Instead an additional tapering factor is applied on the loss coefficient that is equal to unity for $M_1 \geq 1.0$ and zero for $M_1 \leq 0.8$.

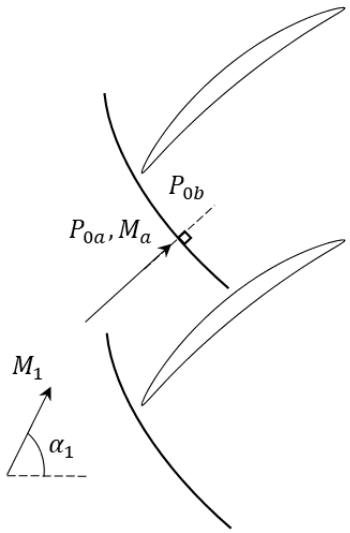

Figure 2.2: Assumed shock-wave formation in a blade-row passage for loss modelling.

Reynolds number effects are considered for the profile and endwall loss correlations when the chord based Reynolds number drops below 10^6. The nominal values for endwall and profile loss estimated by the previously described correlations, are taken

to be valid for $Re \geq 10^6$. Reynolds number effects are included by applying the following corrections to the nominal values.

$$\frac{\omega}{\omega_{Re=10^6}} = \begin{cases} 489.8Re^{-0.5} & Re < 10^5 \\ 13.8Re^{-0.19} & 10^5 \leq Re < 10^6 \\ 1.0 & 10^6 \leq Re. \end{cases} \tag{2.16}$$

It is assumed that the flow is laminar up to $Re = 10^5$ after which it transitions to hydraulically smooth turbulent flow. Beyond 10^6 losses remain unaffected.

2.1.3 Blockage and spanwise mixing

Annulus blockage prediction as implemented in SC90C is largely based on the work by Wright and Miller [11] with an annulus boundary layer model that in turn is heavily inspired by the work of Hirsch [16]. The end purpose of the correlation is to predict area blockage factors B to be used in Eq. 2.5 during the normal equilibrium calculations. For a given quasi-orthogonal the overall blockage for the entire annulus is calculated based on the predicted boundary layer displacement thickness at the hub and the casing yielding

$$B = 1 - \frac{2(r_h\delta_h^* + r_t\delta_t^*)}{r_t^2 - r_h^2}. \tag{2.17}$$

Here δ_h^* and δ_t^* represents the boundary layer displacement thickness at the annulus wall in the normal direction at the hub and the casing respectively. The growth of the displacement thickness from the inlet to the outlet of a blade-row is obtained iteratively by solving a coupled system of equations. In principle the change in momentum thickness $\Delta\theta_{ew}$ from the inlet to the outlet is provided by a model based on 2-dimensional incompressible boundary layer theory with additional empirical terms accounting for the effect of blade forces. By assuming a power-law for the meridional velocity profile inside the boundary layer, Greens entrainment equation [17] can be used to estimate the boundary layer shape factor H at the exit of the blade row for known values at the inlet. From the definition of the shape factor the displacement thickness can then be calculated as $\delta^* = \theta_{ew}/H$.

Spanwise mixing is modelled using the equations of Gallimore [10] implemented using Dunham and Ginders mixing scheme [3]. The model was conceived based on findings by Gallimore and Cumpsty that the main phenomena responsible for spanwise mixing was indeed turbulent diffusion [18]. By the previous assumptions made for the governing equations of the streamline curvature method, both entroy and total enthalpy are conserved in the streamwise direction. As a consequence the exchange of momentum and heat between streamlines is fundamentally neglected. To incorporate the most pronounced effects on the flow field from spanwise mixing, Gallimore derived an energy equation in the meridional direction only allowing for radial transfer of heat between streamlines and shear stresses in the $\theta - z$ plane yielding

$$\frac{\partial s}{\partial m} = \frac{1}{r\rho T V_m}\frac{\partial}{\partial r}\left(rk_t\frac{\partial T}{\partial r}\right) + \frac{\Phi}{\rho T V_m} + \frac{\partial s_e}{\partial m}. \tag{2.18}$$

The entropy increase due to losses imposed by the empirical models described previously, are here calculated separately through $\partial s_e/\partial m$, k_t is the eddy thermal conductivity and the dissipation term Φ depends on the eddy viscosity μ_t and the velocity gradients accordingly

$$\Phi = \mu_t \left[\left(\frac{\partial V_z}{\partial r} \right)^2 + \left(\frac{\partial V_\theta}{\partial r} - \frac{V_\theta}{r} \right)^2 \right] \tag{2.19}$$

Tangential and streamwise momentum equations were derived in a similar fashion - neglecting all shear stresses but the ones in the $\theta - z$ plane arriving at

$$\frac{1}{2r^2} \frac{\partial}{\partial m}(r^2 V_\theta^2) = \frac{V_\theta}{V_m} \left(\frac{F_\theta + E_\theta}{\rho} \right) \tag{2.20}$$

$$\frac{\partial h_0}{\partial m} = T \frac{\partial s}{\partial m} + \frac{1}{2r^2} \frac{\partial}{\partial m}(r^2 V^2) + \frac{F_m}{\rho} + \frac{E_z}{\rho} \cos \phi \tag{2.21}$$

Terms relating the eddy viscosity to the velocity gradients are here denoted E_θ and E_z and are given by the following two expressions.

$$E_\theta = \frac{\partial}{\partial r} \left(\mu_t \left[\frac{\partial V_\theta}{\partial r} - \frac{V_\theta}{r} \right] \right) + \frac{2\mu_t}{r} \left[\frac{\partial V_\theta}{\partial r} - \frac{V_\theta}{r} \right], \tag{2.22}$$

$$E_z = \frac{1}{r} \frac{\partial}{\partial r} \left[\mu_t r \frac{\partial V_z}{\partial r} \right] \tag{2.23}$$

The two additional force terms F_θ and F_m in Eq. 2.20 and 2.21 are added to take into account the change in tangential and meridional velocity over a blade row that are determined without the influence from spanwise turbulent dissipation. It can further be shown that the two force components are geometrically related as follows

$$F_m = F_\theta \frac{V_\theta}{V_m} - F_d, \tag{2.24}$$

where F_d is a drag force in the meridional direction. If there are no spanwise gradients such as in the case of a linear cascade, the drag force can be related to the empirical losses s_e accordingly

$$F_d = \rho T \frac{\partial s_e}{\partial m}. \tag{2.25}$$

The change in tangential velocity as predicted by the correlations described earlier can then be used together with Eq. 2.20 but without the dissipation term E_θ to evaluate the tangential blade force.

What remains in order to close this system of equations is a way to calculate the eddy viscosity μ_t and the eddy thermal conductivity k_t. The eddy viscosity is for this purpose obtained through a mixing parameter introduced by Gallimore defined as

$$\epsilon_{gal} = \frac{\mu_t}{\rho V_z l}, \tag{2.26}$$

where l is the annulus height. For air at close to atmospheric condition a value of $\epsilon_{gal} = 5.6 \times 10^{-4}$ is recommended according the SC90C manual. The eddy thermal conductivity is furthermore specified by the turbulent Prandtl-number $Pr_t = \mu_t c_p / k_t$ and a value of unity was shown to be reasonable for axial compressors [10].

Chapter 3

Summary of Papers

3.1 Paper 1

In Paper 1, an assessment of the degree of uncertainty in matching a cycle performance model to publicly available data for a state-of-the-art commercial aircraft engine was performed. Performance metrics were investigated as well as limitations of inverse engine cycle matching.

3.1.1 Methodology

The study was performed through an iterative process to determine the thermodynamic cycle based on public data for both on-design and off-design points for the GEnx-1B, a two-spool, direct driven, separate flow turbofan intended for medium- to long-range commercial aircraft. The Chalmers in-house gas turbine simulations tool, GESTPAN, wrapped with an external solver was then used to evaluate the engine performance in the obtained points. The solver ensured that the constraints set by the known data were met by the performance model. The uncertainty level of the model matching method was evaluated using the Latin Hyper Cube Sampling technique. The final outcome was an estimation of the design parameters and performance metrics as well as their interdependencies in terms of statistical measures for this inverse design problem.

3.1.2 Summary and discussion

It was observed that the fuel burn performance can be estimated with some degree of confidence, while the prediction of the low-pressure system performance indicated a need for supporting studies on conceptual design and cost. The SFC range variation was estimated at 2.5% of the median, whereas the corresponding FPR range was 4.5%. Using a constant jet-velocity-ratio at TOC resulted in a reduced FPR range of 1.89%, but with little impact on in the SFC range. The absence of a significant trend between the FPR and the resulting polytropic efficiency was attributed to a wide spread in the empirical input model between FPR and the unmatched polytropic efficiency. The fan-face Mach number varied around 4.4% relative to the mean,

which was primarily influenced by the uncertenties in inlet mass flow during take-off. This study highlights the importance of statistical methods during an inverse design procedure. The results showed the limitations of relying solely on public data for conventional thermodynamic matching. Such matching procedure, although valid and important, requires the support from conceptual design, cost and fuel burn studies to accurately estimate the low-pressure system performance metrics with a higher degree of certainty.

3.2 Paper 2

In Paper 2, parametric optimization was applied on a streamline curvature method to assess parameter interdependencies in fan-stage aerothermodynamic performance. Surrogate models, created from the parametric optimization data, were used to support the component-level design space exploration. A subsequent case study was performed, to demonstrate the integration of surrogate models into an engine systems model to evaluate engine weight and specific thrust trade-offs.

3.2.1 Methodology

The parametric optimization was initialized by a latin hypercube sampling of values for stage loading, flow coefficient, rotor aspect ratio, and fan-face Mach number. For each sampling point, a two-objective optimization on a streamline curvature model was performed to determine Pareto optimal designs based on stage polytropic efficiency and blade loading. Using these parameters as independent variables, surrogate models were then generated for polytropic efficiency and rotor solidity. As a second part of the study, the generated model was coupled with a simplified weight model and integrated into an engine performance model. This setup was then used to assess the effect of the fan stage attributes on the trade-off between engine weight and thrust specific fuel consumption, by performing a design space exploration.

3.2.2 Summary and discussion

The trends predicted by the surrogate models could to some extent be justified with physical reasoning and by comparing with literature guidelines. With regard to the choice of blade loading as an optimization objective, this could potentially exclude globally optimal designs, highlighting the need for optimization algorithms that employ unknown preference ordering. Future work could include more geometric features in the interdependency study and the incorporation of Reynolds number effects. This would require expanding the optimization approach in order to increase its sensitivity to geometrical features. The second part of the study highlighted the significance of a multidisciplinary approach when evaluating fan-stage aerothermodynamic performance. When evaluating the trade-off between engine weight and thrust-specific fuel consumption for a high-bypass, low specific thrust turbofan, the ability to predict the rotor solidity of the fan stage for a given average blade loading was shown to be equally important as predicting fan stage efficiency. Extending the

low-order model to include off-design performance effects is considered for future work. This could enable the direct coupling with aircraft design and mission analysis to examine fan parameters impact on operational flexibility.

Chapter 4

Concluding Remarks

4.1 Summary

The contribution of this study was to establish an optimization methodology to support the conceptual design of the fan stage in low-specific thrust turbofans. The work started by developing thermodynamic models of state-of-the-art turbofan engines while relying on public available data. At the same time, the most important fan stage performance and conceptual design parameters were identified to establish the design space for subsequent optimization studies. The second part of the work consisted of developing a low-order reduced model that includes performance features that define the fan stage aerodynamic performance. This model is later inserted into the existing thermodynamic model for the estimation of the higher level of fan-stage parameter interdependency in the early stages of conceptual design.

4.2 Future work

The test cases reported here provided insight into the implication of a few fan stage geometrical features in the fuel burn performance of modern turbofan engines, while limited by the accuracy of the streamline curvature models. Several geometric features not included in the interdependency study for could be of interest to include in future work, such as rotor inlet hub-tip-ratio, rotor and OGV maximum profile thickness at the tip and the hub, and tip clearance.Including the diameter as an independent parameter in order to account for Reynolds number effects and choosing a more representative baseline domain in terms of the hub and the casing contours are additional aspects worth considering. Parameter interdependencies representative for state-of-the-art and future fan technology, would require the high-fidelity method used during the parametric optimization to be sensitive to more geometric features. If the effects from detailed variations in the blade profile shapes should be taken into account, a blade-to-blade solver coupled with a throughflow solver could be justifiable. If 3D features such as lean and sweep are considered important then 3D RANS of the entire blade passage would most likely be required. For the parametric optimization to be computationally feasible in this case without having to sacrifice too much in

terms of the parameter sample size, a surrogate assisted approach would probably be necessary for this purpose as well. Additional considerations for future work includes extending the low-order model to incorporate relevant effects on off-design performance characteristic as well. This could potentially facilitate a direct coupling of the engine model with aircraft design and mission analysis to investigate how fan parameters effect operational flexibility. Validating the stall margin parameter and test different spanwise avergaing. Consider regularization techniques on surrogate models to enforce or encourage convexity or monotonicity in certain dimensions where this could be expected, as means to improve the confidence in the prediction and usability (for gradient based optimization) when the underlying data is noise or from different sources of different quality.

Bibliography

[1] A. J. Wennerstrom, "Low aspect ratio axial flow compressors: Why and what it means," *Trans ASME Journal of Turbomachinery*, vol. 111, no. October 1989, pp. 357–365, 1986, ISSN: 26883627. DOI: 10.4271/861837 (cit. on p. 3).

[2] J. D. Denton, "Throughlow calculations for transonic axial flow turbines," *Journal of Engineering for Gas Turbines and Power*, vol. 100, no. 2, pp. 212–218, 1978, ISSN: 15288919. DOI: 10.1115/1.3446336 (cit. on p. 7).

[3] J. Dunham and R. B. A. Ginder, *A streamline curvature throughflow program for turbomachines*, 1991 (cit. on pp. 7, 13).

[4] R. A. Novak, "Streamline curvature computing procedures for fluid flow problems," *Trans ASME Journal of Engineering for Power*, vol. 89, pp. 478–490, 1967 (cit. on p. 7).

[5] R. A. Novak and R. M. Hearsay, "A nearly three-dimensional intrablade computing system for turbomachinery," *ASME Journal of Engineering for Power*, vol. 99, pp. 154–166, 1977 (cit. on p. 7).

[6] R. H. Aungier, *Axial Flow Compressors: A strategy for aerodynamic design and analysis*. New York: The American Society of Mechanical Engineers, 2003, ISBN: 0-7918-0192-6 (cit. on pp. 8, 10).

[7] J. D. Denton, "The use of a distributed body force to simulate viscous effects in 3D flow calculations," in *ASME 31st International Gas Turbine Confernece and Exhibit*, Dusseldorf, 1986, 86–GT–144 (cit. on p. 9).

[8] R. C. Dean, "On the necessity of unsteady flow in fluid machines," *ASME Journal of Basic Engineering*, vol. 81, pp. 24–28, 1959 (cit. on p. 9).

[9] N. A. Cumpsty, *Compressor aerodynamics*. Essex: Longman Scientific and Technical, 1989, ISBN: 0-470-21334-5 (cit. on pp. 9, 10).

[10] S. J. Gallimore, "Spanwise mixing in multi-stage axial flow compressors. Part II—Throughflow Calculations Including Mixing," *Trans ASME Journal of Turbomachinery*, vol. 108, no. July 1986, pp. 10–16, 1986 (cit. on pp. 9, 13, 14).

[11] P. I. Wright and D. C. Miller, "An improved compressor performance prediction model," in *Proceedings of the Institution of Mechanical Engineers, Turbomachinery: Latest Developments in a Changing Scene*, Mechanical Engineering Publications Limited, 1991, pp. 69–82 (cit. on pp. 10, 11, 13).

[12] D. C. Miller and D. L. Wasdell, "Off-design prediction of compressor blade losses," in *Proceedings of the Institution of Mechanical Engineers, Turbomachinery: Efficiency Prediction and Improvement*, 1987, pp. 249–260 (cit. on p. 10).

[13] S. Lieblein, "Loss and Stall Analysis of Compressor Cascades," *Trans ASME Journal of Basic Engineering*, vol. 81, pp. 387–400, 1959 (cit. on p. 11).

[14] S. Lieblein, F. C. Schwenk, and R. L. Broderick, *Diffusion Factor for Estimating Losses and Limiting Blade Loadings in Axial-flow Compressor Blade Elements, RM E53D01*, Washington, D.C., 1953 (cit. on p. 11).

[15] F. C. Schwenk, G. W. Lewis, and M. J. Hartman, "A Preliminary Analysis of the Wgnitude of Shock Losses in Transonic Compressors," National Advisory Committee for Aeronautics, Washington, Tech. Rep. April, 1957 (cit. on p. 12).

[16] J. De Ruyck and C. Hirsch, "Investigations of an Axial Compressor End-Wall Boundary Layer Prediction Method.," *Trans ASME Journal of Engineering for Power*, vol. 103, pp. 20–33, 1980, ISSN: 04021215 (cit. on p. 13).

[17] J. E. Green, *Application of Heads entrainment method to predict turbulent boundary layers and wakes in compressible flow*, 1972 (cit. on p. 13).

[18] S. J. Gallimore and N. A. Cumpsty, "Spanwise mixing in multi-stage axial compressors: Part I—Experimental Investigation," *Trans ASME Journal of Turbomachinery*, vol. 108, no. July 1986, pp. 2–9, 1985 (cit. on p. 13).